Density functional calculations of nuclear magnetic shieldings using the zeroth-order regular approximation (ZORA) for relativistic effects: ZORA nuclear magnetic resonance.

Wolff, S.K.; Ziegler, T.; van Lenthe, E.; Baerends, E.J.

published in
Journal of Chemical Physics
1999

DOI (link to publisher)
10.1063/1.478680

document version
Publisher's PDF, also known as Version of record

Density functional calculations of nuclear magnetic shieldings using the zeroth-order regular approximation (ZORA) for relativistic effects: ZORA nuclear magnetic resonance

S. K. Wolff and T. Ziegler[a)]
Department of Chemistry, The University of Calgary, Calgary, Alberta, T2N 1N4, Canada

E. van Lenthe and E. J. Baerends
Afdeling Theoretisch Chemie, Scheikundig Laboratorium der Vrije Universiteit De Boelelaan 1083, 1081 HV Amsterdam, The Netherlands

(Received 20 October 1998; accepted 29 December 1998)

We present a new relativistic formulation for the calculation of nuclear magnetic resonance (NMR) shielding tensors. The formulation makes use of gauge-including atomic orbitals and is based on density functional theory. The relativistic effects are included by making use of the zeroth-order regular approximation. This formulation has been implemented and the ^{199}Hg NMR shifts of $HgMe_2$, HgMeCN, $Hg(CN)_2$, HgMeCl, HgMeBr, HgMeI, $HgCl_2$, $HgBr_2$, and HgI_2 have been calculated using both experimental and optimized geometries. For experimental geometries, good qualitative agreement with experiment is obtained. Quantitatively, the calculated results deviate from experiment on average by 163 ppm, which is approximately 3% of the range of ^{199}Hg NMR. The experimental effects of an electron donating solvent on the mercury shifts have been reproduced with calculations on $HgCl_2(NH_3)_2$, $HgBr_2(NH_3)_2$, and $HgI_2(NH_3)_2$. In addition, it is shown that the mercury NMR shieldings are sensitive to geometry with changes for $HgCl_2$ of approximately 50 ppm for each 0.01 Å change in bond length, and 100 ppm for each 10° change in bond angle. [S0021-9606(99)30313-5]

I. INTRODUCTION

The aim of the work presented in this paper has been to use the zeroth-order regular approximation (ZORA)[1–4] to incorporate the effects of relativity into the calculation of nuclear magnetic resonance (NMR) shielding tensors, and to test our implementation of the ZORA NMR by evaluating ^{199}Hg chemical shifts.

The method for calculating the NMR shieldings using ZORA is an extension of the approach of Scheckenbach and Ziegler,[5] and of Wolff and Ziegler,[6] in which the more familiar relativistic Pauli approximation together with density functional theory (DFT) and gauge-including atomic orbitals (GIAO) was used to calculate the NMR shielding tensors.

In the sections that follow we give a brief introduction to ZORA and its relation to the Dirac equation and the Pauli approximation. We then present ZORA expressions for the shielding tensor, and show that the total shielding may be regarded as a sum of three contributions: a paramagnetic contribution, a diamagnetic contribution, and a ''spin–orbit coupling'' contribution. To determine the quality of the ZORA NMR, ^{13}C NMR shieldings and chemical shifts of methyl halides and carbon tetrahalides are calculated and compared to both experiment and NMR shieldings and shifts calculated within the Pauli approximation. Finally, we present calculated ^{199}Hg NMR shieldings and chemical shifts for a variety of mercury compounds, and demonstrate that these shieldings and shifts are sensitive to both geometry and solvent effects.

II. THE ZEROTH-ORDER REGULAR APPROXIMATION (ZORA)

In this section we give a brief introduction to ZORA. For more details the reader is referred to the literature.[1–4]

The one-electron Dirac eigenequation may be written as:

$$\begin{pmatrix} V & c\boldsymbol{\sigma}\cdot\mathbf{p} \\ c\boldsymbol{\sigma}\cdot\mathbf{p} & V-2c^2 \end{pmatrix}\begin{pmatrix} \phi \\ \chi \end{pmatrix} = E\begin{pmatrix} \phi \\ \chi \end{pmatrix}.$$

Here, V is the electrostatic potential energy, c is the speed of light, $\boldsymbol{\sigma}$ is the three-component Pauli spin matrix, $\mathbf{p}$ is the three-component momentum operator, E is the energy, and ϕ and χ are the ''large'' and ''small'' components, respectively.

Each of the large and small components are two-component spinors. We require an eigenequation involving only the large component.

The large and small component are related by $\chi = X\phi$, where

$$X = \frac{1}{2c}\left(1+\frac{E-V}{2c^2}\right)^{-1}\boldsymbol{\sigma}\cdot\mathbf{p}. \tag{1}$$

Accordingly, the small component can be formally eliminated to give the following eigenequation for the large component:

$$(V + c\boldsymbol{\sigma}\cdot\mathbf{p}X)\phi = E\phi.$$

a)Author to whom correspondence should be addressed. Electronic mail: ziegler@ucalgary.ca

However, the Hamiltonian in this equation is not Hermitian, and the resulting eigenfunctions ϕ are not normalized. These problems can be circumvented by introducing the Hermitian Hamiltonian

$$h=(1+X^{\dagger}X)^{1/2}(V+c\boldsymbol{\sigma}\cdot\mathbf{p}X)(1+X^{\dagger}X)^{-1/2}, \tag{2}$$

which affords normalized states. To simplify this Hamiltonian, we can assume that $p^2 \ll 4c^2$ and expand Eq. (2) to get the familiar relativistic Pauli approximation:

$$h^{\mathrm{Pauli}}=V+\frac{p^2}{2}-\frac{p^4}{8c^2}+\frac{\nabla^2 V}{8c^2}+\frac{1}{4c^2}\boldsymbol{\sigma}\cdot(\nabla V\times\mathbf{p}).$$

The problem with this approximation is that in the core region of a heavy atom the assumption that $p^2 \ll 4c^2$ is no longer appropriate, and thus the expansions that lead to the Pauli Hamiltonian are no longer valid in this region. One of the consequences of this is that for heavy atoms a frozen core must be used in order to ensure variational stability.

An alternative approximation to the above Pauli approximation can be obtained by rewriting Eq. (1) as:

$$X=\left(\frac{c}{2c^2-V}\right)\left(1+\frac{E}{2c^2-V}\right)^{-1}\boldsymbol{\sigma}\cdot\mathbf{p}. \tag{3}$$

If we assume $E \ll (2c^2-V)$, then Eq. (3) can be expanded to zeroth order in $E/(2c^2-V)$ to give the zeroth-order regular approximation (ZORA):[1]

$$h^{\mathrm{ZORA}}=\boldsymbol{\sigma}\cdot\mathbf{p}\frac{K}{2}\boldsymbol{\sigma}\cdot\mathbf{p}+V, \tag{4}$$

where

$$K=[1-V/2c^2]^{-1}. \tag{5}$$

In this case the assumption that $E \ll (2c^2-V)$ in the core region, and thus the expansions that lead to the ZORA Hamiltonian, remains valid. As a result, the ZORA Hamiltonian does not suffer from variational instabilities and can be used in all-electron calculations.

ZORA orbital energies can be improved further by introducing a simple scale factor.[3] If

$$h^{\mathrm{ZORA}}\psi_i=E_i^{\mathrm{ZORA}}\psi_i, \tag{6}$$

then the scaled energies $E_i^{\mathrm{scaled}}=\xi_i E_i^{\mathrm{ZORA}}$, where

$$\xi_i=\left(1+\langle\psi_i|\boldsymbol{\sigma}\cdot\mathbf{p}\frac{c^2}{(2c^2-V)^2}\boldsymbol{\sigma}\cdot\mathbf{p}|\psi_i\rangle\right)^{-1}, \tag{7}$$

are in much better agreement with the one-electron Dirac energies.

For a multielectron system the total energy in the scaled ZORA DFT formalism is given by[3]

$$E_{\mathrm{TOT}}^{\mathrm{scaled}}=\sum_i^{N_{\mathrm{occ}}} E_i^{\mathrm{scaled}}-\frac{1}{2}\int\int\frac{\rho(1)\rho(2)}{r_{12}}d1\,d2 + E_{\mathrm{XC}}[\rho]-\int\rho(1)\frac{\delta E_{\mathrm{XC}}[\rho]}{\delta\rho(1)}d1. \tag{8}$$

III. FORMULATION

In the DFT approach that we use to find the ZORA NMR shielding tensors, we make use of a magnetic field dependent ZORA Hamiltonian,

$$h^{\mathrm{ZORA}}(\boldsymbol{\pi})=\boldsymbol{\sigma}\cdot\boldsymbol{\pi}\frac{K}{2}\boldsymbol{\sigma}\cdot\boldsymbol{\pi}+V, \tag{9}$$

where K is defined in Eq. (5), and $\boldsymbol{\pi}=\mathbf{p}+(1/c)\mathbf{A}$, with $\mathbf{A}$ the magnetic vector potential

$$\mathbf{A}=\mathbf{A}_B+\mathbf{A}_\mu=\tfrac{1}{2}\mathbf{B}\times\mathbf{r}+(\boldsymbol{\mu}_Q\times\mathbf{r}_Q)/r_Q^3.$$

Here $\mathbf{B}$ is the external magnetic field, $\boldsymbol{\mu}_Q$ is the nuclear magnetic moment attached to nucleus Q at position $\mathbf{R}_Q$, and $\mathbf{r}_Q=\mathbf{r}-\mathbf{R}_Q$.

Exact solutions of the ZORA equation (9) are independent (up to a phase factor) of the choice of origin of the vector potential for the external magnetic field. While there is a dependency on the gauge of the electrical potential V, which can be solved as discussed in Ref. 3, there is no special problem in the ZORA equation (9) with respect to the dependency on the choice of origin for the vector potential. In finite basis sets there is of course the well known gauge-dependency problem, which is solved by the use of gauge-including atomic orbitals, see below.

The NMR shielding tensor can then be found from the total scaled energy Eq. (8) using

$$\sigma_{kt}=\partial_{B_k}\partial_{\mu_{Q,t}}E_{\mathrm{TOT}}^{\mathrm{scaled}}|_{\mathbf{B}=\boldsymbol{\mu}_Q=0} =\partial_{B_k}\sum_i^{N_{\mathrm{occ}}}\xi_i\left\langle\psi_i(\mathbf{B})\left|\frac{\partial h^{\mathrm{ZORA}}(\boldsymbol{\pi})}{\partial\mu_{Q,t}}\right|_{\boldsymbol{\mu}_Q=0}\psi_i(\mathbf{B})\right\rangle_{\mathbf{B}=0}. \tag{10}$$

In this expression, ξ_i are the scale factors defined as in Eq. (7), σ_{kt} is the shielding tensor component due to the change in the kth component of the magnetic field B_k, and the tth component of the magnetic moment $\mu_{Q,t}$ of nucleus Q. The notations ∂_{B_k} and $\partial_{\mu_{Q,t}}$ denote the partial derivatives with respect to B_k and $\mu_{Q,t}$, respectively. In our formulations we will try to follow closely the notations of Wolff and Ziegler,[6] although we are now using the ZORA Hamiltonian instead of the relativistic Pauli Hamiltonian.

It should be noted that when a magnetic field is introduced, the total energy given by Eq. (8) will be a functional of both the density and the current density. In deriving Eq. (10) from Eq. (8) it is assumed that the total energy is independent of the current, and that the first-order change in the density vanishes. Thus we are using uncoupled DFT to determine the NMR shieldings.[6]

It is straightforward to calculate the derivative with respect to $\mu_{Q,t}$ in the ZORA formalism,

$$\left.\frac{\partial h^{\mathrm{ZORA}}(\boldsymbol{\pi})}{\partial\mu_{Q,t}}\right|_{\boldsymbol{\mu}_Q=0}=h_t^{01}+\sum_{s=1}^{3}B_k h_{kt}^{11}+h_t^{\mathrm{SO}} \tag{11}$$

with

$$h_t^{01}=\frac{K}{2cr_Q^3}(\mathbf{r}_Q\times\mathbf{p})_t+(\mathbf{r}_Q\times\mathbf{p})_t\frac{K}{2cr_Q^3}, \tag{12}$$

$$h_{kt}^{11}=\frac{K}{4c^2r_Q^3}(\mathbf{r}_Q\cdot\mathbf{r}\,\delta_{kt}-r_{Q_k}r_t), \tag{13}$$

$$h_t^{\mathrm{SO}} = \sigma_t \nabla \cdot \left(\frac{K}{2cr_Q^3} \mathbf{r}_Q \right) - \nabla_t \left(\frac{K}{2cr_Q^3} \boldsymbol{\sigma} \cdot \mathbf{r}_Q \right). \tag{14}$$

In order to evaluate the expression in Eq. (10) we also need to know the spinors $\psi_i(\mathbf{B})$ up to first order in the magnetic field. We first solve the ZORA equation, without magnetic field

$$h^{\mathrm{ZORA}} \psi_i = \left(V + \boldsymbol{\sigma} \cdot \mathbf{p} \frac{K}{2} \boldsymbol{\sigma} \cdot \mathbf{p} \right) \psi_i = E_i^{\mathrm{ZORA}} \psi_i . \tag{15}$$

This solution can be written in terms of real atomic basis functions φ_ν,

$$\psi_i = \sum_\nu^N \sum_{\gamma=\alpha,\beta} d_{\nu i}^\gamma \varphi_\nu \gamma, \tag{16}$$

with complex coefficients $d_{\nu i}^\gamma$, and spin function γ, which is either α or β spin.

Next we calculate the solutions of the ZORA equation including the external magnetic field $\mathbf{B}$ up to first order,

$$h^{\mathrm{ZORA}}(\mathbf{B}) \psi_i(\mathbf{B}) = E_i(\mathbf{B}) \psi_i(\mathbf{B}), \tag{17}$$

where $h^{\mathrm{ZORA}}(\mathbf{B})$ up to first order in $\mathbf{B}$ is

$$\begin{aligned} h^{\mathrm{ZORA}}(\mathbf{B}) &= V + \boldsymbol{\sigma} \cdot \left(\mathbf{p} + \frac{1}{c} \mathbf{A}_B \right) \frac{K}{2} \boldsymbol{\sigma} \cdot \left(\mathbf{p} + \frac{1}{c} \mathbf{A}_B \right) \\ &= V + \boldsymbol{\sigma} \cdot \mathbf{p} \frac{K}{2} \boldsymbol{\sigma} \cdot \mathbf{p} + \frac{K}{4c} \mathbf{B} \cdot (\mathbf{r} \times \mathbf{p}) + \mathbf{B} \cdot (\mathbf{r} \times \mathbf{p}) \frac{K}{4c} \\ &\quad + \frac{K}{2c} \boldsymbol{\sigma} \cdot \mathbf{B} + \boldsymbol{\sigma} \cdot \mathbf{B} \left(\mathbf{r} \cdot \nabla \frac{K-1}{4c} \right) \\ &\quad - \boldsymbol{\sigma} \cdot \mathbf{r} \left(\mathbf{B} \cdot \nabla \frac{K-1}{4c} \right). \end{aligned} \tag{18}$$

Gauge-including atomic orbitals (GIAOs) are used to ensure that the calculated results do not depend on the gauge origin of the magnetic vector potential $\mathbf{A}_B$. The basis functions now depend on the external magnetic field as:

$$\varphi_\nu(\mathbf{B}) = \exp[-(i/2c)(\mathbf{B} \times \mathbf{R}_\nu) \cdot \mathbf{r}] \varphi_\nu . \tag{19}$$

It is convenient to introduce an auxiliary basis set with basis functions Φ_j,

$$\Phi_j = \sum_\nu^N \sum_{\gamma=\alpha,\beta} d_{\nu j}^\gamma \varphi_\nu(\mathbf{B}) \gamma, \tag{20}$$

in order to write the solution $\psi_i(\mathbf{B})$ in terms of these basis functions:

$$\psi_i(\mathbf{B}) = \sum_j^N u_{ji} \Phi_j . \tag{21}$$

Thus up to first order in the external magnetic field,

$$\begin{aligned} \psi_i(\mathbf{B}) &= \Phi_i + \sum_j^N \mathbf{B} \cdot \boldsymbol{u}_{ji}^1 \Phi_j \\ &= \psi_i + \sum_\nu^N \sum_{\gamma=\alpha,\beta} \frac{i}{2c} d_{\nu i}^\gamma \mathbf{B} \cdot (\mathbf{r} \times \mathbf{R}_\nu) \varphi_\nu \gamma + \sum_j^N \mathbf{B} \cdot \boldsymbol{u}_{ji}^1 \psi_j . \end{aligned} \tag{22}$$

Using first order perturbation theory (FOPT) the k component of the expansion coefficients u_{ij} is

$$u_{ii}^{1,k} = -\tfrac{1}{2} S_{ii}^{1,k}, \tag{23}$$

$$u_{ji}^{1,k} = \frac{F_{ji}^{1,k} - \epsilon_i^0 S_{ji}^{1,k}}{\epsilon_i^0 - \epsilon_j^0} \quad \text{for } i \neq j, \tag{24}$$

with

$$\begin{aligned} S_{ji}^{1,k} &= \partial_{B_k} \langle \Phi_j | \Phi_i \rangle_{\mathbf{B}=0} \\ &= \frac{i}{2c} \sum_{\mu,\nu}^N \langle \varphi_\mu | [\mathbf{r} \times (\mathbf{R}_\nu - \mathbf{R}_\mu)]_k | \varphi_\nu^0 \rangle \\ &\quad \times \left(\sum_{\gamma=\alpha,\beta} d_{\mu j}^{\gamma *} d_{\nu i}^\gamma \right), \end{aligned} \tag{25}$$

$$\begin{aligned} F_{ji}^{1,k} &= \partial_{B_k} \langle \Phi_j | h^{\mathrm{ZORA}}(\mathbf{B}) | \Phi_i \rangle_{\mathbf{B}=0} \\ &= \sum_{\mu,\nu}^N \langle \varphi_\mu | \frac{K}{4c} [\mathbf{r}_\mu \times \mathbf{p}]_k + [\mathbf{r}_\nu \times \mathbf{p}]_k \frac{K}{4c} | \varphi_\nu \rangle \left(\sum_{\gamma=\alpha,\beta} d_{\mu j}^{\gamma *} d_{\nu i}^\gamma \right) \\ &\quad + \sum_{\mu,\nu}^N \langle \varphi_\mu | \frac{iV}{2c} [\mathbf{r} \times (\mathbf{R}_\nu - \mathbf{R}_\mu)]_k + \mathbf{p} \cdot \frac{iK}{4c} [\mathbf{r} \times (\mathbf{R}_\nu - \mathbf{R}_\mu)]_k \mathbf{p} | \varphi_\nu \rangle \\ &\quad \times \left(\sum_{\gamma=\alpha,\beta} d_{\mu j}^{\gamma *} d_{\nu i}^\gamma \right) + \sum_{\mu,\nu}^N \sum_{\gamma',\gamma=\alpha,\beta} d_{\mu j}^{\gamma *} d_{\nu i}^{\gamma'} \langle \varphi_\mu \gamma | \boldsymbol{\sigma} \cdot \left[\nabla \left(i \frac{K-1}{4c} [\mathbf{r} \times (\mathbf{R}_\nu - \mathbf{R}_\mu)]_k \right) \times \mathbf{p} \right] | \varphi_\nu \gamma' \rangle \\ &\quad + \sum_{\mu,\nu}^N \sum_{\gamma',\gamma=\alpha,\beta} d_{\mu j}^{\gamma *} d_{\nu i}^{\gamma'} \langle \varphi_\mu \gamma | \frac{1}{2c} \boldsymbol{\sigma}_k - i \frac{K-1}{4c} \boldsymbol{\sigma}_k \mathbf{r}_\mu \cdot \mathbf{p} + \mathbf{p} \cdot \mathbf{r}_\nu \boldsymbol{\sigma}_k i \frac{K-1}{4c} | \varphi_\nu \gamma' \rangle \\ &\quad + \sum_{\mu,\nu}^N \sum_{\gamma',\gamma=\alpha,\beta} d_{\mu j}^{\gamma *} d_{\nu i}^{\gamma'} \langle \varphi_\mu \gamma | i \frac{K-1}{4c} \boldsymbol{\sigma} \cdot \mathbf{r}_\mu p_k - p_k \boldsymbol{\sigma} \cdot \mathbf{r}_\nu i \frac{K-1}{4c} | \varphi_\nu \gamma' \rangle, \end{aligned} \tag{26}$$

for the first-order overlap matrix $S_{ji}^{1,k}$ and for the first-order DFT matrix $F_{ji}^{1,k}$, respectively. Related relations can be found in Ref. 7 for the calculation of the g tensor, which parametrizes the Zeeman interaction, the interaction of the (effective) electronic spin of a paramagnetic molecule of interest with an external magnetic field.

A. Expressions for the shielding tensor

Following Ref. 6, the NMR shielding tensor is written as a sum of three contributions,

$$\sigma_{kt}=\sigma_{kt}^{d}+\sigma_{kt}^{p}+\sigma_{kt}^{\mathrm{SO}}, \tag{27}$$

where σ_{kt}^{d} is the diamagnetic contribution to the shielding tensor given by

$$\sigma_{kt}^{d}=\sum_{i}^{N_{\mathrm{occ}}}\xi_i\sum_{\mu,\nu}^{N}\langle\varphi_\mu|\frac{1}{2}h_{\mu,kt}^{11}+\frac{1}{2}h_{\nu,kt}^{11}+R_{\mu\nu,kt}^{01}|\varphi_\nu\rangle \times\left(\sum_{\gamma=\alpha,\beta}d_{\mu i}^{\gamma *}d_{\nu i}^{\gamma}\right), \tag{28}$$

σ_{kt}^{p} is the paramagnetic contribution given by

$$\begin{aligned}\sigma_{kt}^{p}=&\sum_{i}^{N_{\mathrm{occ}}}\xi_i\sum_{\mu,\nu}^{N}\langle\varphi_\mu|(i/2c)(\mathbf{R}_\nu\times\mathbf{R}_\mu)h_t^{01}|\varphi_\nu\rangle\\ &\times\left(\sum_{\gamma=\alpha,\beta}d_{\mu i}^{\gamma *}d_{\nu i}^{\gamma}\right)-\sum_{i,j}^{N_{\mathrm{occ}}}\xi_i S_{ji}^{1,k}\sum_{\mu,\nu}^{N}\langle\varphi_\mu|h_t^{01}|\varphi_\nu\rangle\\ &\times\left(\sum_{\gamma=\alpha,\beta}d_{\mu i}^{\gamma *}d_{\nu i}^{\gamma}\right)+2\mathrm{Re}\left[\sum_{i}^{N_{\mathrm{occ}}}\xi_i\sum_{a}^{N_{\mathrm{vir}}}\right.\\ &\left.\times u_{ai}^{1,k}\sum_{\mu,\nu}^{N}\langle\varphi_\mu|h_t^{01}|\varphi_\nu\rangle\left(\sum_{\gamma=\alpha,\beta}d_{\mu i}^{\gamma *}d_{\nu a}^{\gamma}\right)\right],\end{aligned} \tag{29}$$

and $\sigma_{kt}^{\mathrm{SO}}$ is the spin–orbit contribution given by

$$\begin{aligned}\sigma_{kt}^{\mathrm{SO}}=&\sum_{i}^{N_{\mathrm{occ}}}\xi_i\sum_{\mu,\nu}^{N}\sum_{\gamma',\gamma=\alpha,\beta}d_{\mu i}^{\gamma *}d_{\nu i}^{\gamma'}\langle\varphi_\mu\gamma|(i/2c)\\ &\times[\mathbf{r}\times(\mathbf{R}_\nu-\mathbf{R}_\mu)]_k h_t^{\mathrm{SO}}|\varphi_\nu\gamma'\rangle\\ &-\sum_{i,j}^{N_{\mathrm{occ}}}\xi_i S_{ji}^{1,k}\sum_{\mu,\nu}^{N}\sum_{\gamma',\gamma=\alpha,\beta}d_{\mu j}^{\gamma *}d_{\nu i}^{\gamma'}\langle\varphi_\mu\gamma|h_t^{\mathrm{SO}}|\varphi_\nu\gamma'\rangle\\ &+2\mathrm{Re}\left[\sum_{i}^{N_{\mathrm{occ}}}\xi_i\sum_{a}^{N_{\mathrm{vir}}}u_{ai}^{1,k}\sum_{\mu,\nu}^{N}\sum_{\gamma',\gamma=\alpha,\beta}\right.\\ &\left.\times d_{\mu i}^{\gamma *}d_{\nu a}^{\gamma'}\langle\varphi_\mu\gamma|h_t^{\mathrm{SO}}|\varphi_\nu\gamma'\rangle\right].\end{aligned} \tag{30}$$

In Eqs. (27)–(30)

$$\begin{aligned}h_{\nu,kt}^{11}&=\frac{K}{4c^2r_Q^3}(\mathbf{r}_Q\cdot\mathbf{r}_\nu\delta_{kt}-r_{Q_k}r_{\nu_t}),\\ R_{\mu\nu,kt}^{01}&=\frac{iK}{4c^2r_Q^3}[\mathbf{r}_\nu\times(\mathbf{R}_\nu-\mathbf{R}_\mu)]_k(\mathbf{r}_Q\times\mathbf{p})_t\\ &\quad+(\mathbf{r}_Q\times\mathbf{p})_t\frac{iK}{4c^2r_Q^3}[\mathbf{r}_\mu\times(\mathbf{R}_\nu-\mathbf{R}_\mu)]_k,\end{aligned} \tag{31}$$

h_t^{01} and h_t^{SO} were defined in Eqs. (12) and (14), respectively, and ξ_i is the scale factor defined in Eq. (7). Note that in deriving Eq. (30), it has been assumed that the ξ_i are independent of the magnetic field.

In the above formulas, N_{occ} is the number of occupied molecular orbitals (MOs), N_{vir} the number of virtual orbitals, and N is the number of atomic orbitals. The indices i and j are used for the occupied orbitals, a is an index for the virtual orbitals, μ and ν are indices for the basis functions, γ and γ' are indices for the α and β spins, $k=1,2,3$ is the magnetic field component, and $t=1,2,3$ is the nuclear magnetic moment component.

B. The similarity of the ZORA NMR formulation to the standard NMR formulation

The principle difference between the ZORA NMR expressions for the operators of Eqs. (12)–(14), and standard expressions[5,6,8–11] is the appearance of the factor K, defined as in Eq. (5). Setting $K=1$, the expressions for the ZORA NMR operators h^{01} and h^{11}, given by Eqs. (12) and (13), become the familiar nonrelativistic NMR paramagnetic and diamagnetic expressions. Furthermore, noting that Eq. (14) can be rewritten as

$$\begin{aligned}K\left[\sigma_t\left(\frac{8\pi}{3}\delta(\mathbf{r}_Q)-\frac{\sigma_t}{r_Q^3}\right)+\frac{3\boldsymbol{\sigma}\cdot\mathbf{r}_Q r_{Q,t}}{r_Q^5}\right]\\ +\sigma_t\nabla K\cdot\left(\frac{\mathbf{r}_Q}{r_Q^3}\right)-\nabla_t K\left(\frac{\mathbf{r}_Q\cdot\boldsymbol{\sigma}}{r_Q^3}\right),\end{aligned} \tag{32}$$

and setting $K=1$, the following expression is obtained:

$$\sigma_t\left(\frac{8\pi}{3}\delta(\mathbf{r}_Q)-\frac{\sigma_t}{r_Q^3}\right)+\frac{3\boldsymbol{\sigma}\cdot\mathbf{r}_Q r_{Q,t}}{r_Q^5}.$$

This is the Fermi-contact term plus spin–dipolar operators of Ballard *et al.*[8] Thus at $K=1$, the ZORA NMR expressions for the operators reduce to the standard expressions.

For a point charge, $V\sim-1/r$. In this case, $K\approx0$ near the point charge, but $K\approx1$ away from the point charge. Thus, one could say that near a nucleus, the ZORA spin–dipolar parts differ from the more familiar parts, but away from the nucleus, it is essentially the same. In the ZORA NMR formulation the Fermi-contact term does not arise from the first term in Eq. (32), since $K\approx0$ near the point charge, but arises from the last two terms in this equation. This interesting feature of the (regular approximated) relativistic hyperfine interaction was already observed by Harriman.[12]

IV. IMPLEMENTATION

Implementation of the above formulation was carried out within the Amsterdam Density Functional (ADF) package.[13] This package was developed by Baerends[14] and Ravenek.[15] ADF makes extensive use of the numerical integration scheme developed by te Velde.[16] This integration scheme makes it possible to evaluate all required atomic matrix elements accurately. The ZORA part of ADF was developed by van Lenthe *et al.*[1]

TABLE I. ZORA vs Pauli spin–orbit (PSO) calculated ^{13}C NMR shieldings and shifts (in ppm) using experimental geometries.

Molecule[a]	ZORA σ^{cal}	ZORA δ^{cal}	PSO σ^{cal}	PSO δ^{cal}	δ^{expt}	ZORA diff[n]	PSO diff[n]
TMS[b]	186.11	0.0	185.20	0.0	0.0	0.0	0.0
CH_4[c]	194.78	−8.67	195.47	−10.27	−1.8[j]	6.9	8.5
CH_3F[d]	109.36	76.75	109.75	75.45	75.7[j]	1.1	0.3
CH_3Cl[c]	157.51	28.60	158.32	26.88	25.2[j]	3.4	1.7
CH_3Br[e]	175.39	10.72	179.21	5.99	9.7[j]	1.0	3.7
CH_3I[c]	204.25	−18.14	219.36	−34.16	−22.0[j]	3.9	12.2
CF_4[f]	53.56	132.55	53.93	131.27	119.9[l]	12.6	11.4
CCl_4[g]	64.01	122.10	65.62	119.58	96.7[k]	25.4	22.9
CBr_4[h]	191.30	−5.19	243.72	−58.52	−28.5[k]	23.3	30.0
CI_4[i]	473.06	−286.95	427.05	−241.85	−292.0[m]	5.1	50.1
Abs. mean						9.2	15.6

[a]Basis set V used except for molecules containing iodine in which case basis set IV was used.
[b]Optimized in ADF using gradient correction PW91.
[c]Reference 31.
[d]Reference 32.
[e]Reference 33.
[f]Reference 34.
[g]Reference 35.
[h]Reference 36.
[i]Reference 37.
[j]Reference 38.
[k]Reference 39.
[l]Reference 40.
[m]Reference 41.
[n]''diff'' is $|\delta^{cal}-\delta^{expt}|$.

The ZORA NMR routines for calculating the shielding tensors were programmed by the authors of this paper. The NMR routines use the MO coefficients of an ADF ZORA calculation. The matrix elements are evaluated over atomic orbitals by numerical integration, and then transformed to molecular orbitals.

The program was tested by various means, one of which involved calculating the ^{13}C NMR of various carbon-containing molecules using both the ZORA NMR program and a Pauli spin–orbit (PSO) quasirelativistic NMR program developed earlier by the authors of this paper.[6] A discussion of the data is presented shortly.

V. COMPUTATIONAL DETAILS

The ZORA NMR chemical shifts were evaluated by the GIAO ZORA method presented in this work. Where experi-

TABLE II. Calculated ^{199}Hg NMR shielding constants and shifts (in ppm) using experimental geometries.

Molecule[a]	σ^{para}	σ^{dia}	σ^{SO}	σ^{cal}	δ^{cal}	δ^{expt}	Solvent	diff[e]
$HgMe_2$	−4055.71	9613.79	2461.91	8 019.99	0	0	Neat	0
HgMeCN	−3271.79	9614.29	2538.51	8 881.02	−861.03	−766[b]	THF	95
HgMeCl	−3134.98	9615.11	2482.50	8 962.63	−942.64	−861[c]	THF	82
HgMeBr	−3214.88	9613.30	2690.14	9 088.14	−1068.15	−915[c]	CH_2Cl_2	153
HgMeI	−3558.69	9617.52	2985.10	9 043.93	−1024.91	−1097[c]	CH_2Cl_2	72
$Hg(CN)_2$	−2768.95	9614.50	2898.39	9 743.94	−1723.95	−1386[b]	THF	338
$HgCl_2$	−2688.76	9615.56	2649.09	9 575.88	−1555.89	−1518.6[d]	THF	37
$HgBr_2$	−2569.31	9611.72	3662.02	10 704.43	−2684.44	−2213.1[d]	THF	471
HgI_2	−3033.18	9620.51	4938.71	11 526.03	−3506.04	−3447.0[d]	THF	59
$HgCl_2(NH_3)_2$	−3350.63	9617.21	2838.93	9 105.51	−1085.52	−1279.5[d]	py	194
$HgBr_2(NH_3)_2$	−3402.08	9614.21	3665.61	9 877.71	−1857.72	−1622.2[d]	py	236
$HgI_2(NH_3)_2$	−3731.50	9620.94	4966.29	10 855.74	−2835.75	−2355.1[d]	py	481
Abs. mean								163[f]

[a]Basis set V used throughout. See Table III for geometries.
[b]Reference 49.
[c]Reference 44.
[d]Reference 43 converted as in Wrackmeyer and Contreras (Ref. 20).
[e]''diff'' is $|\delta^{cal}-\delta^{expt}|$.
[f]Excluding the ammonia-containing molecules.

TABLE III. Experimental geometries used in Table II. Lengths in Å, angles in degrees.

Molecule	Geometry[a]	State	Method
$HgMe_2$[b]	r(Hg–C)=2.083, r(C–H)=1.106 (a.)	Gas	Electron diff.
HgMeCN[c]	r(Hg–Me)=2.05, r(Hg–CN)=2.08, r(C–N)=1.14, r(C–H)=0.98 (av.), ∠(Hg–C–H)=111 (av.)	Solid	X-ray diff.
HgMeCl[d]	r(Hg–C)=2.061, r(Hg–Cl)=2.282, r(C–H)=1.10 (a.), ∠(H–C–H)=110.7 (a.)	Gas	Microwave
HgMeBr[d]	r(Hg–C)=2.074, r(Hg–Br)=2.406, r(C–H)=1.10 (a.), ∠(H–C–H)=110.7 (a.)	Gas	Microwave
HgMeI[e]	r(Hg–C)=2.087, r(Hg–I)=2.528, r(C–H)=1.10 (a.), ∠(H–C–H)=110.7 (a.)	Gas	Microwave
$Hg(CN)_2$[f]	r(Hg–C)=2.015, r(C–N)=1.137, not linear	Solid	Neutron diff.
$HgCl_2$[g]	r(Hg–Cl)=2.252	Gas	Electron diff.
$HgBr_2$[h]	r(Hg–Br)=2.41	Gas	Electron diff.
HgI_2[i]	r(Hg–I)=2.554	Gas	Electron diff.

[a]Molecules are linear unless otherwise stated. Where bond lengths or angles are not reported in the references, they were quasirelativistically optimized in ADF with gradient correction PW91. ''av.'' = averaged, ''a.'' = assumed.
[b]Reference 27.
[c]Reference 45.
[d]Reference 46.
[e]Reference 47.
[f]Reference 48.
[g]Reference 28.
[h]Reference 26.
[i]Reference 29.

mental geometries were not used, the geometries were optimized using a quasirelativistic method. The direct optimization by ZORA is still under development.

Special basis sets were employed in all ZORA calculations. These all-electron basis sets use Slater type orbitals (STOs), and are double ζ in the core, triple ζ in the valence, and have one or two polarization functions added. A basis set with one polarization function added will be referred to as a ''IV basis set,'' and a basis set with two polarization functions added will be referred to as a ''V basis set''—this corresponds to the designations given to these sets in the ADF package.

For the quasirelativistic calculations, basis sets of the same type as the ZORA IV basis sets were used, but with the addition of frozen cores. For the geometry optimizations, the cores of Hg, I, Br, Cl, N and C were frozen up to and including $4d$, $4p$, $3p$, $2p$, $1s$, and $1s$, respectively. For the ^{13}C PSO NMR calculations, no frozen core was used for C.

The functionals used in the calculation of the molecular orbitals were the local-density approximation (LDA) of Vosko, Wilk, and Nusair[17] augmented with the gradient correction due to Perdew and Wang[18] (which will be referred to as the PW91 gradient correction).

TABLE IV. Geometries used for the mercury ammonia halides of Table V. Lengths are in Å, angles in degrees.

Molecule	Geometry[a]
$HgCl_2(NH_3)_2$	r(Hg–Cl)=2.375, r(Hg–N)=2.47, ∠(Cl–Hg–Cl)=150.0 (a.), ∠(Cl–Hg–N)=98.74 (opt.)
$HgBr_2(NH_3)_2$	r(Hg–Br)=2.497, r(Hg–N)=2.45, ∠(Br–Hg–Br)=151.0, ∠(Br–Hg–N)=98.76 (opt.)
$HgI_2(NH_3)_2$	r(Hg–I)=2.665, r(Hg–N)=2.43, ∠(I–Hg–I)=143.0, ∠(I–Hg–N)=100.93 (opt.)

[a]The geometries of $HgCl_2(py)_2$, $HgBr_2(py)_2$ and $HgI_2(py)_2$ from the paper by Persson (Ref. 19) were used. Where bond lengths or angles are not reported in the reference, they were quasirelativistically optimized in ADF with gradient correction PW91. ''a.'' = assumed, ''opt.'' = optimized.

In calculating the NMR results of Tables I and II experimental geometries have been used. References for the geometries of the carbon compounds of Table I are given in that table. For the mercury compounds of Table II, the geometries together with references are given in Table III. Most of the geometries are gas phase, measured by either microwave spectroscopy or electron diffraction. In some references, not all geometry parameters are given. In these cases, the geometry used for the NMR calculations was fixed as far as possible using the experimental parameters, and then all undetermined parameters were optimized quasirelativistically in ADF using the PW91 gradient correction.

For the geometries of $HgCl_2(NH_3)_2$, $HgBr_2(NH_3)_2$, and $HgI_2(NH_3)_2$ in Table II the experimental geometries[19] of $HgCl_2(py)_2$, $HgBr_2(py)_2$, and $HgI_2(py)_2$ were used to fix the Hg–halide bond length and angle, and the Hg–N bond length, and the rest of the structure was geometry optimized. The geometries used are summarized in Table IV.

Tables of the experimental ^{199}Hg NMR shifts with respect to $HgMe_2$ are given in a review paper by Wrackmeyer and Contreras.[20] We have included specific references to these experimental shifts in our tables.

VI. CALCULATED ^{13}C NMR SHIELDINGS

The ^{13}C NMR shieldings and chemical shifts have been calculated for the molecules CH_4, CH_3F, CH_3Cl, CH_3Br, CH_3I, CF_4, CCl_4, CBr_4, and CI_4 using both the ZORA NMR program and the PSO quasirelativistic NMR program developed earlier by the authors of this paper.[6] The principle purpose for doing these calculations was to provide an additional check that the ZORA NMR program was performing properly.

It should be noted that spin–orbit coupling (a relativistic effect) is known to add an important contribution to the ^{13}C shieldings (as well as other atom shieldings) when heavy atoms such as Br and I are bonded directly to the NMR probe atom. This contribution is the result of spin–orbit coupling and the magnetic field inducing a spin density in the molecule which can be detected at the NMR probe atom through a Fermi-contact interaction. For a detailed discussion of the physical mechanism of the spin–orbit contribution to NMR shieldings the reader is referred to the paper of Kaupp *et al.*[21]

TABLE V. Experimental ^{199}Hg shifts (in ppm) in various solvents relative to $HgMe_2$.

Molecule	δ^{expt}	Solvent
$HgMe_2$	−108.2[a]	DMSO
	−94.6[a]	Pyridine
	−75.6[a]	THF
	−11.2[a]	CCl_4
	+5.3[a]	Hexane
$HgCl_2$	−1501.6[a]	DMSO
	−1279.5[b]	Pyridine
	−1518.6[b]	THF
$HgBr_2$	−2062.1[b]	DMSO
	−1622.2[b]	Pyridine
	−2213.1[b]	THF
HgI_2	−3119.0[b]	DMSO
	−2355.1[b]	Pyridine
	−3447.0[b]	THF
MeHgCl	−810[c]	$CDCl_3$
	−813[c]	C_6H_6
	−847.9[a]	DMSO
	−861[c]	THF

[a]Reference 42.
[b]Reference 43 converted as in Wrackmeyer and Contreras (Ref. 20).
[c]Reference 44.

The ^{13}C NMR data is presented in Table I. Both the ZORA and PSO NMR shifts agree well for molecules containing atoms not heavier than Cl. This is to be expected as in these molecules relativistic effects are small. The deviation between the ZORA and PSO NMR shifts increases for the molecules containing the atoms Br and I. This is to be expected as relativistic effects are known to be large in these atoms, and ZORA incorporates the effects of relativity more completely than does PSO.

A comparison to experiment is also shown in Table I, and the absolute differences (diff) to experiment as well as the average of the absolute differences is presented. For this set of molecules, the average difference of the ZORA NMR from experiment is 9.2 ppm compared to 15.6 ppm for the PSO NMR. These results help to confirm that the ZORA NMR program is calculating the shieldings correctly according to the formulations.

VII. ^{199}Hg NMR SHIFTS

We shall in the following sections apply the new ZORA NMR formulation to the calculation of ^{199}Hg NMR shifts. To our knowledge, the only other detailed calculations of mercury shifts have been carried out by Nakatsuji.[22] They calculated the shifts of mercury chloride, bromide, and iodide, using the mercury chloride as the reference. We also calculate the shieldings for these molecules but in addition consider $HgMe_2$, which is currently one of the most used internal references,[20] as well as the molecules HgMeCN, $Hg(CN)_2$, HgMeCl, HgMeBr, and HgMeI.

As will be discussed shortly, the experimental mercury shifts are sensitive to solvent. Therefore we also calculate shifts of the roughly tetrahedral molecules[19] $HgCl_2(NH_3)_2$, $HgBr_2(NH_3)_2$, and $HgI_2(NH_3)_2$, where the ammonia molecules simulate the effect of a strong electron donating solvent.

The following range of ^{199}Hg NMR is worth noting:[20]

$$-3500 \quad \text{for } [HgI_4]^{2-} < {}^{199}\text{Hg} < +1700 \quad \text{for } [Hg(SiR_3)_4]^{2-} \quad (\text{in ppm}),$$

Thus the range of mercury NMR is approximately 5000 ppm.

A. The sensitivity of experimental ^{199}Hg shifts to the solvent

We consider here the sensitivity of the experimental ^{199}Hg shifts to the solvent. Table V illustrates the experimentally observed solvent dependence of the ^{199}Hg shifts.[20]

The mercury molecules that we examine in this work are linear in the gas phase. In an electron donating solvent this is not necessarily the case. For instance, the experiments of Persson *et al.*[19] have established that in pyridine solutions of mercury halides, two pyridine molecules coordinate to the mercury atom forming a roughly tetrahedral complex. For mercury chloride, this results in a Cl–Hg–Cl angle of about 150°.[19] Experimental evidence indicates that complexes of similar geometry will also form in other electron donating solvents.[23]

The degree to which these molecules are bent in an electron donating solvent is proportional to the coordinating ability of the solvent. In another study, Persson *et al.*[23] used spectroscopic evidence to show that the coordinating ability of methanol, DMSO, and pyridine to mercury dihalides increases in the order methanol < DMSO < pyridine, and that the halide–Hg–halide angle decreases correspondingly. For mercury chloride, the Cl–Hg–Cl angle was estimated to be about 175° in methanol, 162° in DMSO, and 154° in pyridine. THF coordinates even more weakly than methanol.[23] Based on these observations, it is reasonable to assume that for the solvents THF, DMSO, and pyridine, the mercury halides are closest to their gas phase nature in THF, and furtherest from their gas phase nature in pyridine.

In our calculations we have attached two ammonia molecules to the mercury halides to simulate the effect of a strong coordinating solvent. According to Persson *et al.*,[23] ammonia coordinates more strongly than pyridine, to the point that in liquid ammonia, only mercury iodide does not dissociate.

B. The experimental geometries of the mercury compounds

Examination of the experimental bond lengths of the mercury dihalides[24] reveals that the difference in the Hg–halide bond length between solid and gas phase may be as much 0.1 Å. Furthermore, variation in the literature values[25] for the Hg–halide bond length in the gas phase is as much as 0.05 Å. Admittedly, some of this literature is old (approximate years 1930–1950). The most recent structure determination of $HgBr_2$ appears to be from 1959 where Akishin *et al.*[26] estimated the Hg–Br distance to be 2.41 Å. Our calculations show that a change in the bond length of 0.05 Å can affect the mercury shifts of the halides to the order of 100–200 ppm, depending on the halide.

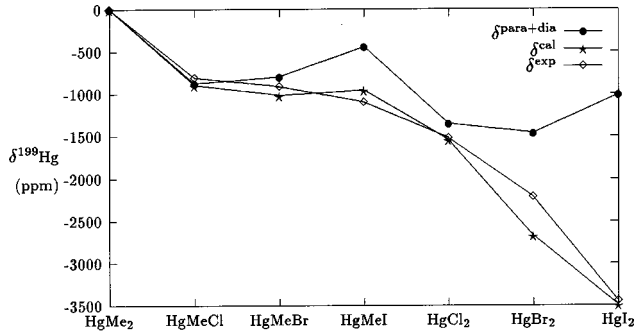

FIG. 1. Calculated and experimental ^{199}Hg NMR shifts (in ppm) using experimental geometries.

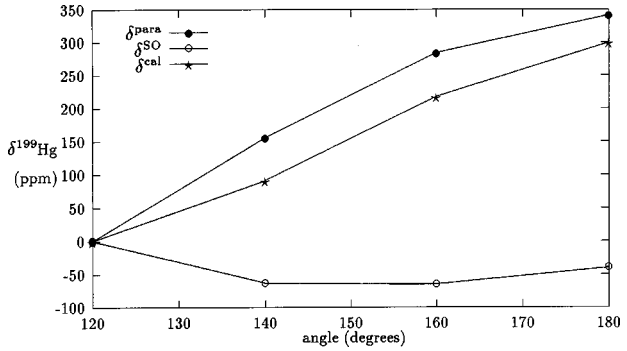

FIG. 3. Calculated ^{199}Hg NMR shielding changes (in ppm) with change in Cl–Hg–Cl angle (in degrees) for $HgCl_2$.

For the gas phase the most recent values of the Hg–ligand bond lengths for $HgMe_2$, $HgCl_2$, $HgBr_2$, and HgI_2 are 2.083 Å,[27] 2.252 Å,[28] 2.41 Å,[26] and 2.554 Å.[29] If we wish to consider optimized geometries, the inclusion of both correlation and relativisitic effects are essential in obtaining reasonable agreement to these experimental geometries. For instance, Kaupp and Schnering[30] have shown that for $HgCl_2$ the calculated bond length using the nonrelativistic Hartree–Fock approach is 2.441 Å, whereas with relativity included an improved bond length of 2.313 Å is obtained. With a relativistic MP2 calculation a bond length of 2.293 Å is obtained. Our best quasirelativistic DFT optimization on $HgCl_2$ affords a Hg–Cl bond distance of 2.289 Å, which is 0.037 Å longer than the experimental estimate. Our calculations reveal that such a discrepancy can introduce an uncertainty of approximately a 150 ppm change in the shift.

VIII. CALCULATED ^{199}Hg NMR SHIELDINGS

In the tables that follow σ^{para}, σ^{dia}, and σ^{SO} are the contributions to the total calculated isotropic shielding, σ^{cal}, from the paramagnetic, diamagnetic and spin–orbit coupling Hamiltonians, respectively. Furthermore, δ^{cal} and δ^{expt} are the calculated and experimental chemical shifts, respectively. Here the calculated shift is evaluated as

$$\delta^{sample} = \sigma^{HgMe_2} - \sigma^{sample}.$$

Finally, ''diff'' is the absolute difference between δ^{cal} and δ^{expt}, and ''solvent'' is the solvent used in the NMR experiment.

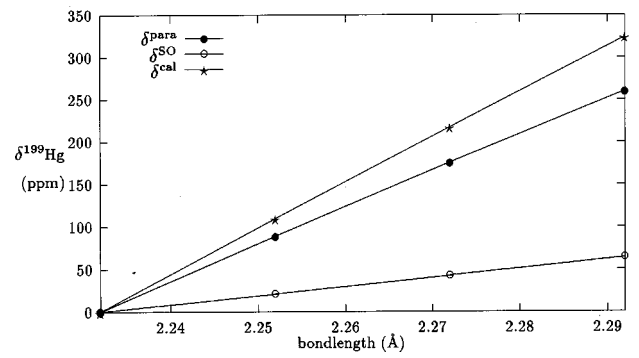

FIG. 2. Calculated ^{199}Hg NMR shielding changes (in ppm) with change in bond length (in Å) for linear $HgCl_2$.

All shifts are in ppm, all bond lengths are in angströms (Å), and all angles are in degrees (°).

A. ^{199}Hg NMR using experimental geometries

Table II presents ^{199}Hg ZORA NMR shieldings and shifts calculated at experimental gas phase and crystal geometries.

For the molecules $HgMe_2$, HgMeCN, $Hg(CN)_2$, HgMeCl, HgMeBr, HgMeI, $HgCl_2$, $HgBr_2$, and HgI_2 the average absolute deviation between experiment and theory is 163 ppm, corresponding to 3% of the total range for the ^{199}Hg chemical shift of the investigated mercury species. The largest error of 500 ppm is observed for $HgBr_2$. It is not clear whether the large deviation for $HgBr_2$ is due to uncertainties in the geometry or deficiencies in the ZORA NMR scheme.

Figure 1 illustrates graphically how the calculated NMR shifts of the halide-containing molecules compare with experiment. It is clear that the trends in the calculated NMR are in qualitative agreement with experiment. The plot of $\delta^{para+dia}$ in Fig. 1 shows the importance of the spin–orbit coupling contribution in getting the correct trend.

Figures 2 and 3 underline the dependence of the calculated chemical shifts on the molecular geometry. Figure 2 clearly shows the linear relationship between the calculated shifts and variations in the bond length for $HgCl_2$. A change of 0.01 Å in bond length results in a change of approximately 50 ppm for the calculated shifts. The change in the paramagnetic contribution is much larger than the change in the spin–orbit coupling contribution. The diamagnetic contribution is effectively constant and has not been shown in the plot. Figure 3 shows the relationship between the calculated shift of $HgCl_2$ and the Cl–Hg–Cl bond angle. The relationship is roughly linear with a change of 100 ppm for every 10° change in the bond angle.

In Fig. 4 we illustrate graphically how the calculated NMR shifts compare with experiment for the molecules $HgCl_2$, $HgCl_2(NH_3)_2$, $HgBr_2$, $HgBr_2(NH_3)_2$, HgI_2, and $HgCl_2(NH_3)_2$. Note that for $HgCl_2$, $HgBr_2$, and HgI_2 the experimental solvent was THF. Furthermore, the calculated mercury shifts of $HgCl_2(NH_3)_2$, $HgBr_2(NH_3)_2$, and $HgCl_2(NH_3)_2$ are being compared to the experimental shifts of the mercury dihalides in pyridine, or in other words, to the experimental shifts of the complexes $HgCl_2(py)_2$, $HgBr_2(py)_2$, and $HgCl_2(py)_2$. Thus, although quantitative

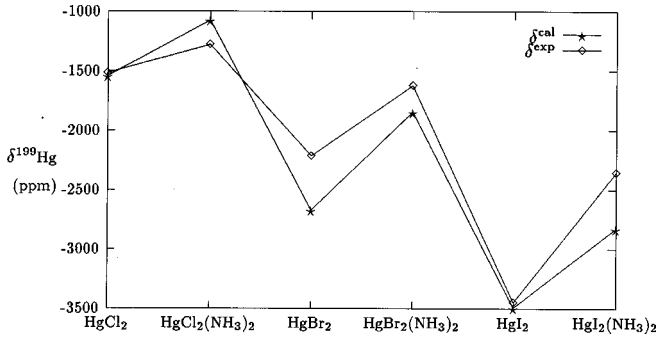

FIG. 4. Calculated and experimental ^{199}Hg NMR shifts (in ppm) using experimental geometries.

agreement should not be expected here, the qualitative experimental trends are reproduced by the calculation.

Lewis bases such as ammonia and pyridine will on coordination with mercury halides influence the chemical ^{199}Hg shift by bending the X–Hg–X angle and interacting directly with the mercury center. We can assess the individual contributions by starting with linear $HgCl_2$ for which the chemical shift is -1555.89 ppm. Now distorting $HgCl_2$ to the conformation it has in $HgCl_2(NH_3)_2$ affords a shift of -2140.98 ppm. The further coordination of ammonia to yield $HgCl_2(NH_3)_2$ affords a shift of -1085.52 ppm. It is thus clear that the direct interaction between mercury and NH_3 is the major factor responsible for the difference in the ^{199}Hg shift between $HgCl_2(NH_3)_2$ and $HgCl_2$.

B. ^{199}Hg NMR using optimized bond lengths

Table VI presents ^{199}Hg ZORA NMR shieldings and shifts relative to $HgMe_2$, calculated using optimized geometries. Note that we have included the molecule $Hg(SiH_3)_2$.

Here the differences between calculated and experimental shifts are disappointingly large as a result of the deviations between optimized and experimentally determined geometries. For HgI_2 the optimized bond length is 0.08 Å longer that the experimental value, which translates into a difference of 900 ppm between shifts calculated with optimized and experimental structures, respectively, see Tables II and VI. The optimized structures for the chloride-containing compounds are closer to the experimental estimates with the result that the shifts calculated at these geometries are more similar than for the iodine systems.

TABLE VI. Calculated ^{199}Hg NMR shielding constants and shifts (in ppm) using optimized geometries.

Molecule[a]	r(Hg–L)[b]	σ^{cal}	δ^{cal}	δ^{expt}	diff[e]
$Hg(SiH_3)_2$	2.5083	7 648.57	+442.92	+196.0[c]	247
$HgMe_2$	2.1013	8 091.49	0	0	0
$HgCl_2$	2.2889	9 774.02	−1682.53	−1518.6[d]	164
$HgBr_2$	2.4380	10 952.13	−2860.60	−2213.1[d]	648
HgI_2	2.6334	12 500.57	−4409.08	−3447.0[d]	962
$HgCl_2(NH_3)_2$	···	9 476.07	−1384.58	−1279.5[d]	105
$HgBr_2(NH_3)_2$	···	10 613.60	−2522.11	−1622.2[d]	900
$HgI_2(NH_3)_2$	···	12 132.93	−4041.44	−2355.1[d]	1686

[a]Basis set V used throughout.
[b]The optimized Hg–Si, Hg–C, Hg–Cl, Hg–Br, and Hg–I bond lengths in Å; quasirelativistically optimized in ADF using the PW91 gradient correction.
[c]Reference 50.
[d]Reference 43 converted as in Wrackmeyer and Contreras (Ref. 20). See Table II for solvents.
[e]''diff'' is $|\delta^{cal} - \delta^{expt}|$.

IX. CONCLUSIONS

We have presented a new method for the calculation of NMR shielding tensors. The method is based on DFT with GIAOs as basis functions and includes relativistic effects by using the ZORA scheme due to van Lenthe *et al.*[1–4] This formulation has been implemented and the ^{199}Hg NMR shifts of $HgMe_2$, $Hg(CN)_2$, HgMeCN, HgMeCl, HgMeBr, HgMeI, $HgCl_2$, $HgBr_2$, and HgI_2 have been calculated using both experimental and optimized geometries.

Using experimental geometries, good qualitative agreement with experiment is obtained, and quantitatively the calculated results deviate from experiment on average by 163 ppm, which is approximately 3% of the total range of ^{199}Hg NMR.

In addition, it has been shown that the mercury NMR shieldings of $HgCl_2$ depend linearly on the bond length with a change of approximately 50 ppm for each 0.01 Å change in bond length. A roughly linear relationship was also found between the shift and the X–Hg–Y bond angle with a change of 100 ppm for each incremental decrease in the bond angle by 10°. The strong dependence of calculated shifts on the structure puts high demands on the accuracy of optimized geometries if they are to be used in quantitative shift calculations.

The experimental effects of an electron donating solvent on the mercury shifts have been reproduced with calculations on $HgCl_2(NH_3)_2$, $HgBr_2(NH_3)_2$, and $HgI_2(NH_3)_2$. The coordinating electron donating solvent forces the mercury dihalide to bend and the bonds to stretch, thus affecting the mercury shieldings. In addition the direct interaction of the electron donating solvent with the mercury atom also affects the shieldings. Both factors are important in dertermining the correct shieldings.

ACKNOWLEDGMENTS

We are grateful to Dr. G. Schreckenbach for helping test the ZORA NMR routines. This work has been supported by the National Sciences and Engineering Research Council of Canada (NSERC). We thank the donors of the Petroleum Research Fund, administered by the American Chemical Society (Grant No. ACS-PRF 31205-AC3), for further support of this research.

[1] E. van Lenthe, E. J. Baerends, and J. G. Snijders, J. Chem. Phys. **99**, 4597 (1993).
[2] R. van Leeuwen, E. van Lenthe, E. J. Baerends, and J. G. Snijders, J. Chem. Phys. **101**, 1272 (1994).
[3] E. van Lenthe, E. J. Baerends, and J. G. Snijders, J. Chem. Phys. **101**, 9783 (1994).
[4] A. J. Sadlej, J. G. Snijders, E. van Lenthe, and E. J. Baerends, J. Chem. Phys. **102**, 1758 (1995).
[5] G. Schreckenbach and T. Ziegler, J. Phys. Chem. **99**, 606 (1995).
[6] S. K. Wolff and T. Ziegler, J. Chem. Phys. **109**, 895 (1998).

[7] E. van Lenthe, P. E. S. Wormer, and A. van der Avoird, J. Chem. Phys. **107**, 2488 (1997).
[8] C. C. Ballard, M. Hada, H. Kaneko, and H. Nakatsuji, Chem. Phys. Lett. **254**, 170 (1996).
[9] V. G. Malkin, O. L. Malkina, and D. R. Salahub, Chem. Phys. Lett. **261**, 335 (1996).
[10] G. Schreckenbach and T. Ziegler, Int. J. Quantum Chem. **61**, 899 (1997).
[11] H. Fukui, Magn. Reson. Rev. **11**, 205 (1987).
[12] J. E. Harriman, *Theoretical Foundations of Electron Spin Resonance* (Academic, New York, 1978).
[13] Amsterdam Density Functional (ADF), Release 2.0.4, Theoretical Chemistry, Vrije Universiteit, De Boelelaan 1083, 1081 HV Amsterdam, The Netherlands; http://www.scm.com/SCM/
[14] E. J. Baerends, D. E. Ellis, and P. Ros, Chem. Phys. **2**, 41 (1973); E. J. Baerends and P. Ros, *ibid.* **2**, 52 (1973); E. J. Baerends, Ph.D. thesis, Free Univesity, Amsterdam, 1973; E. J. Baerends and P. Ros, Int. J. Quantum Chem., Symp. **12**, 169 (1978).
[15] W. Ravenek, in *Algorithms and Applications on Vector and Parallel Computers*, edited by H. J. J. te Riele, T. J. Dekker, and H. A. van de Horst (Elsevier, Amsterdam, 1987).
[16] P. M. Boerrigter, G. te Velde, and E. J. Baerends, Int. J. Quantum Chem. **33**, 87 (1988); G. te Velde, Ph.D. thesis, Free University, Amsterdam, 1990; G. te Velde and E. J. Baerends, Int. J. Quantum Chem. **99**, 84 (1992).
[17] S. H. Vosko, L. Wilk, and M. Nusair, Can. J. Phys. **58**, 1200 (1980).
[18] J. P. Perdew, J. A. Chevary, S. H. Vosko, K. A. Jackson, M. R. Pederson, D. J. Singh, and C. Fiolhais, Phys. Rev. B **46**, 6671 (1992).
[19] I. Persson, M. Sandström, P. L. Goggin, and A. Mosset, J. Chem. Soc. Dalton Trans. **1985**, 1597.
[20] B. Wrackmeyer and R. Contreras, in *Annual Reports on NMR Spectroscopy*, edited by G. A. Webb (Academic, New York, 1994), Vol. 24.
[21] M. Kaupp, O. L. Malkina, V. G. Malkin, and P. Pyykkö, Chem.-Eur. J. **4**, 118 (1998).
[22] H. Nakatsujis, M. Hada, H. Kaneko, and C. C. Ballard, Chem. Phys. Lett. **255**, 195 (1996).
[23] I. Persson, M. Sandström, and P. L. Goggin, Inorg. Chim. Acta **129**, 183 (1987).
[24] G. J. Grant, in *Encyclopedia of Inorganic Chemistry*, edited by R. B. King (Wiley, New York, 1994), Vol. 4.
[25] *Tables of Interatomic Distances and Configuration in Molecules and Ions*, edited by L. E. Sutton, D. G. Jenkin, A. D. Mitchell, and L. C. Cross (The Chem. Soc., London, 1958).
[26] P. A. Akishin, V. P. Spiridonov, and A. N. Khodchenkov, Zh. Fiz. Khim. **33**, 20 (1959).
[27] K. Kashiwabara, S. Konaka, T. Iijima, and M. Kimura, Bull. Chem. Soc. Jpn. **46**, 407 (1973).
[28] K. Kashiwabara, S. Konaka, and M. Kimura, Bull. Chem. Soc. Jpn. **46**, 410 (1973).
[29] V. P. Spiridonov, A. G. Gershikov, and B. S. Butayev, J. Mol. Struct. **52**, 53 (1979).
[30] M. Kaupp and H. Georg von Schnering, Inorg. Chem. **33**, 2555 (1994).
[31] J. L. Duncan, J. Mol. Struct. **22**, 225 (1974).
[32] D. F. Eggers, Jr., J. Mol. Struct. **31**, 367 (1976).
[33] G. Graner, J. Mol. Spectrosc. **90**, 394 (1981).
[34] S. Brodersen, J. Mol. Spectrosc. **145**, 331 (1991).
[35] Y. Morino, Y. Nakamura, and T. Iijima, J. Chem. Phys. **32**, 643 (1960).
[36] H. Thomassen and K. Hedberg, J. Mol. Struct. **240**, 151 (1990).
[37] S. Pohl, Z. Kristallogr. **159**, 211 (1982).
[38] H. Spiesecke and W. G. Schneider, J. Chem. Phys. **35**, 722 (1961).
[39] W. M. Litchman and D. M. Grant, J. Am. Chem. Soc. **90**, 1400 (1968).
[40] R. A. Demarco, W. B. Fox, W. B. Moniz, and S. A. Sojka, J. Magn. Reson. **18**, 522 (1975).
[41] O. W. Howrath and R. J. Lynch, Mol. Phys. **16**, 431 (1968).
[42] M. A. Sens, N. K. Wilson, P. D. Ellis, and J. D. Odom, J. Magn. Reson. **19**, 323 (1975).
[43] P. Peringer, Inorg. Chim. Acta **39**, 67 (1980).
[44] P. L. Goggin, R. J. Goodfellow, and N. W. Hurst, J. Chem. Soc. Dalton Trans. **1978**, 561.
[45] J. C. Mills, H. S. Preston, and C. H. L. Kennard, J. Organomet. Chem. **14**, 33 (1968).
[46] W. Gordy and J. Shiridan, J. Chem. Phys. **22**, 92 (1954).
[47] C. Feige and H. Hartmann, Z. Naturforsch. A **22**, 1286 (1967).
[48] R. C. Seccombe and C. H. L. Kennard, J. Organomet. Chem. **18**, 243 (1969).
[49] P. L. Goggin, R. J. Goodfellow, D. M. McEwan, A. J. Griffiths and K. Kessler, J. Chem. Res. (M) 2315 (1979).
[50] S. Cradock, E. A. V. Ebsworth, N. S. Hosmane, and K. M. MacKay, Angew. Chem. Int. Ed. Engl. **14**, 167 (1975).